International Journal of Smart Grid (IJSmartGrid)
https://www.ijsmartgrid.org/ Online ISSN: 2602-439X
A. Berrim et al., Vol. 10, No. 1, March, 2026 Research Article

Enhancing Power Quality in Grid- Connected PV Systems Using New Integral Backstepping Control Validated via PIL Co-Simulation

Ali Berrim*, Moussaoui Abdelkrim*, Zellouma Laid **, Houssam Eddine Ghadbane*‡, Habib Benbouhenni ***

*Laboratoire de Génie Électrique de Guelma (LGEG), Université 8 Mai 1945, Guelma 24000, Algeria.

**LEVRES Laboratory, Department of Electrical Engineering, University of El Oued, 39000, Algeria.

*** Department of Electrical Engineering, Faculty of Technology, Hassiba Benbouali University of Chlef, B.P 78C Ouled Fares, Chlef 02180, Algeria

(berrim.ali@univ-guelma.dz, moussaoui.abdelkrim@univ-guelma.dz, Zellouma13@yahoo.fr, ghadbane.houssameddine@univ-guelma.dz, habib0264@gmail.com)

‡Corresponding Author;24000, Tel:+213 657155158,

ghadbane.houssameddine@univ-guelma.dz

Received: 25.07.2025 Accepted: 10.12.2025

Abstract- In the context of the growing global demand for clean and sustainable energy, advanced control strategies for renewable energy systems play a crucial role in improving efficiency, reliability, and grid integration. This paper addresses these challenges by proposing a novel nonlinear integral backstepping control (NIBC) approach for a grid-connected photovoltaic (PV) system with dual functionality. The proposed control scheme is designed to regulate the maximum power point (MPP), current, and DC-link voltage loops, ensuring a stable DC bus voltage while enabling continuous and optimal energy extraction from the PV array. By incorporating power exchange rules with the utility grid into the energy management strategy, effective DC bus voltage regulation is achieved under varying operating conditions. The proposed approach enhances grid power quality by maintaining low harmonic distortion, fast dynamic response, high power factor, and strong robustness, even in the presence of nonlinear loads. Furthermore, the system's performance is evaluated under fluctuating solar irradiation to demonstrate the effectiveness and resilience of the control strategy. To validate its practical feasibility, a Processor-in-the-Loop (PIL) co-simulation using a C2000 LaunchXL-F28379D digital signal processing (DSP) platform is conducted, highlighting the potential of the proposed method to support the reliable and efficient integration of renewable energy sources into modern power grids.

Keywords Grid connected photovoltaic system, double function, nonlinear integral backstepping controller.

1. Introduction

In recent years, the increasing need for electrical energy has put significant amounts of pressure on traditional methods to generate energy, which predominantly rely on fossil fuels such as coal, diesel, and natural gas. These conventional sources, while widely used, are increasingly being recognized for their high costs, inefficiency, and, more critically, their adverse environmental impact. The environmental consequences of continued reliance on such

Cite this article as: A. Berrim, M. Abdelkrim, Z. Laid, H.E. Ghadbane, and H. Benbouhenni, "Enhancing Power Quality in Grid-Connected PV Systems Using New Integral Backstepping Control Validated via PIL Co-Simulation" *International Journal of Smart Grid (ijSmartGrid)*, Vol. 10, No. 1, pp. 48-59, March, 2026.

energy sources, notably the emission of greenhouse gases, exacerbate global warming and climate change. As the world grapples with these challenges, the focus has shifted toward sustainable and renewable energy sources that not only address the rising energy demands but also minimize environmental harm [1-5]. Among the renewable energy technologies, photovoltaic (PV) systems stand out due to their cost-effectiveness, ease of implementation, and environmental benefits [6-8]. PV systems harness solar energy and convert it directly into electricity, offering a pollution-free and sustainable solution for energy generation. The integration of PV systems into the electrical grid, however, introduces several power quality issues, particularly due to the nonlinear characteristics of loads connected to the grid. These issues, including harmonic distortions, reactive power, and fluctuations in active power, can severely affect grid stability and efficiency [9-13].

Various maximum power point tracking (MPPT) techniques have been created because of the nonlinear power-voltage properties of PV panels, from basic extremum-seeking algorithms like Perturb and Observe (P&O) to more sophisticated controllers like as sliding mode controllers (SMC), proportional integral (PI) controller, adaptive controls, neural networks (NN), and fuzzy logic [14-17]. Often, without needing a thorough mathematical model of the PV system, these sophisticated techniques provide greater efficiency and durability. To get the best outcomes, however, they rely heavily on expertise and trial adjustment.

Heuristic global optimisation methods like particle swarm optimisation (PSO) and genetic algorithms (GA) are more efficient for complicated situations like partial shading, guaranteeing convergence to the global maximum power point [18]. Often implemented and validated via MATLAB simulations, other sophisticated nonlinear control techniques—including third-order SMC technique, nonlinear backstepping control (NBC), and their combinations—have been suggested to enhance robustness, dynamic response, and power quality [19].

Despite the advances, challenges remain, such as control complexity, dependency on accurate system modeling, tuning difficulties due to numerous gains, and the presence of steady-state errors (SSEs). To overcome these, integral actions and hybrid control strategies are integrated into controllers, though at the expense of increased implementation complexity.

Shunt active power filter (SAPF) has become crucial for harmonic correction as nonlinear loads impairing power quality are increasingly used; they operate in parallel with the grid to preserve sinusoidal source currents [20-22]. Usually, control techniques for PV-based SAPFs include voltage-oriented control (VOC) and direct power control (DPC), each having its own benefits and trade-offs regarding complexity, dynamic responsiveness, and sensitivity to parameter changes [23]. Improvements, such as space vector pulse width modulations (SV-PWM), have been created to stabilise switching frequencies and enhance general system performance [24].

This paper uses backstepping control to govern the DC-DC boost converter and hence maximise the power drawn from the PV generator. The reference value for the duty cycle of the DC-DC converter is given by two nonlinear integral backstepping controls (NIBCs) controlling the voltage and current of the PV generator. Moreover, backstepping control is used to manage the harmonic currents of the parallel active power filter (PAPF) and also the DC link capacitor voltage. Using the extracted solar power, the control approach for the PV-PAPF system is designed to meet the load requirements. Thus, taking into account the nonlinear load's reactive power consumption and power factor. We used PIL co-simulation to assess the system's operation. The results demonstrate the overall effectiveness of the system.

2. System Description and Modeling

Fig. 1 illustrates the overall configuration and control scheme of the PV-SAPF system, divided into two main sections: the power section and the control section. The power section consists of a voltage source inverter (VSI), a capacitive energy storage circuit on the DC side, and an output filter on the AC side. The control section includes a method for identifying perturbed currents, a DC-link voltage regulator that manages the energy storage component, and a controller for the injected currents.

2.1. SAPF Modeling

In the a-b-c-phase reference frame, the following equations characterise the SAPF's behaviour:

$$\frac{d}{dt}\begin{bmatrix} i_{fa} \\ i_{fb} \\ i_{fc} \end{bmatrix} = -\frac{1}{L_f}\begin{bmatrix} R_f & 0 & 0 \\ 0 & R_f & 0 \\ 0 & 0 & R_f \end{bmatrix}\begin{bmatrix} i_{fa} \\ i_{fb} \\ i_{fc} \end{bmatrix} - \begin{bmatrix} v_{fa} \\ v_{fb} \\ v_{fc} \end{bmatrix} + \begin{bmatrix} v_a \\ v_b \\ v_c \end{bmatrix}$$

$$\frac{dV_{dc}}{dt} = \frac{1}{C_{dc}}(S_a i_{fa} + S_b i_{fb} + S_c i_{fc}) \quad (1)$$

The AC side voltages and currents of the shunt active power filter are represented by $v_{fa,b,c}$ and $i_{fa,b,c}$, respectively. The common coupling voltage point is denoted by $v_{a,b,c}$. where L_f stands for the filter's output inductance and R_f for its resistance. The control signals for the voltage source inverter are denoted by $S_i, i = a, b, c$, and V_{dc} refers to the capacitor C_{dc} voltage.

In the synchronous reference frame, the mathematical model of the shunt active power filter is provided by:

$$\begin{cases} \frac{di_{fd}}{dt} = -\frac{1}{L_f}\left(R_f i_{fd} - v_{fd} + v_d\right) - L_f w. i_{fd} \\ \frac{di_{fq}}{dt} = -\frac{1}{L_f}\left(R_f i_{fq} - v_{fq} + v_q\right) - L_f w. i_{fq} \\ \frac{dV_{dc}}{dt} = \frac{1}{C_{dc}} i_{dc} \end{cases} \quad (2)$$

In the synchronous reference frame, $v_{fd,q}$ and $i_{fd,q}$ denote the SAPF voltages and currents, respectively, while v_d and v_q represent the voltages at the point of common coupling. Additionally, the current flowing through the capacitor C_{dc} is indicated.

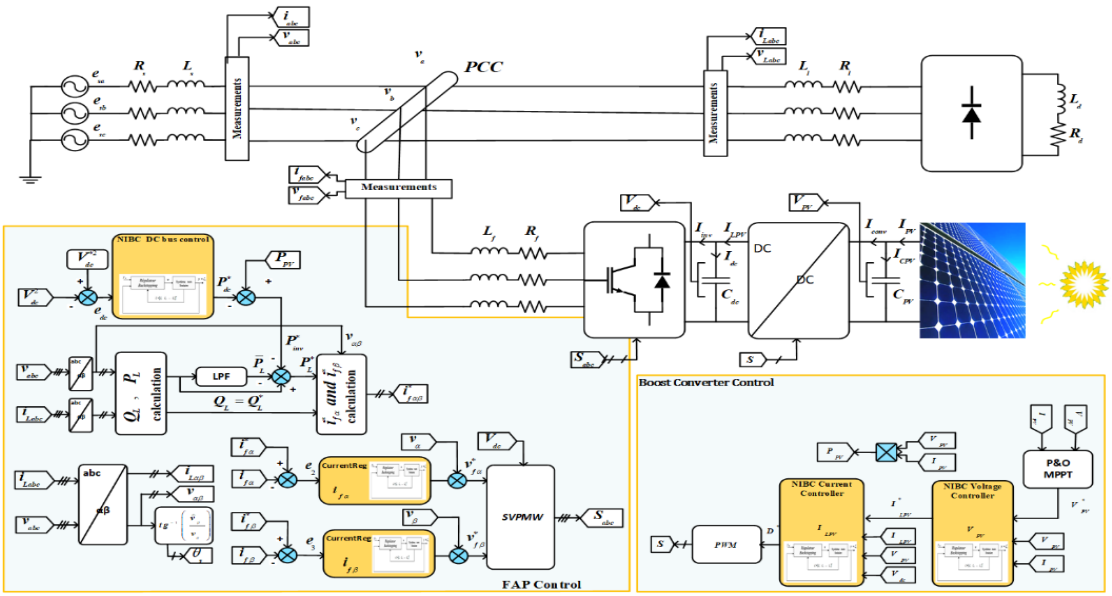

Fig. 1. The proposed control method block diagram.

3. NIBC for the PV- SAPF System

This section implements a backstepping control approach to regulate the DC-DC boost converter, with the objective of maximizing energy extraction from the PV source. Two NIBC controllers are employed to adjust the reference duty cycle of the converter by controlling both the voltage and current of the PV array. Additionally, backstepping techniques are utilized to manage the harmonic currents in the SAPF and to maintain the DC bus voltage.

Using the extracted solar power, adjusting for power factor, and the nonlinear load's reactive power consumption, the control strategy for the PV- SAPF system is meant to satisfy the load demand.

Figure 1 shows the control diagram in the stationary reference frame employing backstepping regulators for the PV-SAPF system.

3.1. *Control Strategy on the FAP Side*

The squared DC bus voltage $V_{dc}^2$and its reference V_{dc}^{2*} are compared in Figure 1. The result is used to feed the error to a backstepping controller. The reference active power $P_{dc}^*$is supplied by the voltage controller's output. Based on instantaneous p-q theory, the compensation powers are computed. To obtain the average powers, a 4th-order low-pass filter is applied. The oscillating powers are determined by subtracting these average values from the corresponding instantaneous active and reactive powers.

3.1.1. Design of the NIBC on the PAPF side

Here, the FAP controllers are synthesised using the backstepping control approach. A breakdown of the full FAP model forms the basis for the construction of the backstepping controllers. For this purpose, system (5) is partitioned into the following three phases:

- **Phase 1**

The derivative of the DC bus voltage can be extracted from Equation (3).

$$\frac{dV_{dc}}{dt} = \frac{P_{dc}}{V_{dc}C_{dc}} \tag{3}$$

In this phase, described by Equation (3), the voltage $V_{dc}$is the output variable, the control variable is the instantaneous active power P_{dc}^*.

- **Phase 2**

The voltage $v_{f\alpha}^*$ in the second stage defined by Equation (4) is selected as the control variable; the current $i_{f\alpha}$ is seen as the output variable.

$$\frac{di_{f\alpha}}{dt} = -\frac{R_f}{L_f}i_{f\alpha} + \frac{v_{f\alpha}^*}{L_f} - \frac{\hat{v}_\alpha}{L_f} \tag{4}$$

- **Phase 3**

In this phase, the control and output variables are respectively represented as $v_{f\beta}^*$ and $i_{f\beta}$:

$$\frac{di_{f\beta}}{dt} = -\frac{R_f}{L_f}i_{f\beta} + \frac{v_{f\beta}^*}{L_f} - \frac{\hat{v}_\beta}{L_f} \tag{5}$$

3.1.2. Design of the NIBC DC bus voltage

The DC bus voltage is controlled to a reference value using a backstepping controller so that it remains at a desired constant value, while compensating for inverter losses.

The tracking error variable z_1 is defined as follows, as this control aims to establish the power reference at the terminals of the DC bus capacitor.

$$z_1 = V_{dc}^* - V_{dc} \tag{6}$$

The first phase provides the error z_1 dynamics as follows:

$$\dot{z}_1 = \dot{V}_{dc}^* - \dot{V}_{dc} = \dot{V}_{dc}^* - \frac{P_{dc}^*}{V_{dc}C_{dc}} \tag{7}$$

We select the Lyapunov candidate function as:

$$V_1 = \frac{1}{2}z_1^2 \tag{8}$$

Function (8) derivative is given by:

$$\dot{V}_1 = z_1\left(\dot{V}_{dc}^* - \frac{P_{dc}^*}{V_{dc}C_{dc}}\right) \tag{9}$$

A negative derivative of the Lyapunov function is required to guarantee system stability. Picking the derivative z_1 of as follows will do this:

$$\dot{z}_1 = -k_1 z_1 \tag{10}$$

Where k_1 represents a gain positive.

Accordingly, the control law is expressed in Equation (11), and its corresponding control structure is illustrated in Fig. 2.

$$P_{dc}^* = V_{dc}C_{dc}\left(\dot{V}_{dc}^* + k_1 z_1\right) \tag{11}$$

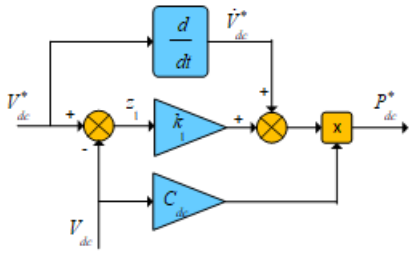

Fig. 2. Control schematic for DC bus voltage regulation.

3.1.3. Synthesis of the NIBC current $i_{f\alpha}$ regulator

The following analysis focuses on the design of the current $i_{f\alpha}$ NIBC controller, formulated from the second part of Equation (1).

The tracking error variable z_2 is expressed as:

$$z_2 = i_{f\alpha}^* - i_{f\alpha} \tag{12}$$

The error z_2's dynamic is defined as:

$$\dot{z}_2 = i_{f\alpha}^* - \left(-\frac{R_f}{L_f}i_{f\alpha} + \frac{v_{f\alpha}^*}{L_f} - \frac{\hat{v}_\alpha}{L_f}\right) \tag{13}$$

It is decided that the Lyapunov candidate function will be:

$$V_2 = \frac{1}{2}z_2^2 \tag{14}$$

The function's derivative Equation (14) is stated as:

$$\dot{V}_2 = z_2\left(i_{f\alpha}^* - \left(-\frac{R_f}{L_f}i_{f\alpha} + \frac{v_{f\alpha}^*}{L_f} - \frac{\hat{v}_\alpha}{L_f}\right)\right) \tag{15}$$

Choosing the derivative z_2 of as guarantees system stability:

$$\dot{z}_2 = -k_2 z_2 \tag{16}$$

Where $k_2$is a gain positive.

Thus, the resulting regulation rule is defined by Equation (17), and its associated schematic is depicted in Fig. 3.

$$v_{f\alpha}^* = L_f i_{f\alpha}^* + L_f k_2 z_2 + R_f i_{f\alpha} + \hat{v}_\alpha \tag{17}$$

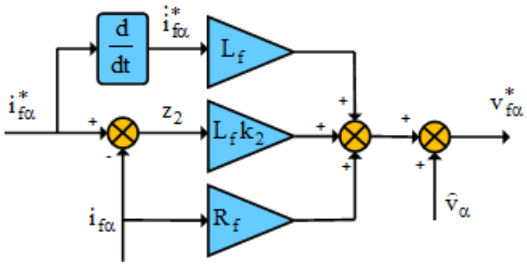

Fig. 3. Schematic of the NIBC control of current $i_{f\alpha}$

3.1.4. Design of the NIBC for current $i_{f\beta}$

The NIBC's design for current $i_{f\beta}$, defined by the third phase specified by Equation (5), is examined as follows:

The tracking error variablez_3 is structured as follows:

$$z_3 = i_{f\beta}^* - i_{f\beta} \tag{18}$$

The error dynamics $z_3$are supplied by:

$$\dot{z}_3 = i_{f\beta}^* - \left(-\frac{R_f}{L_f}i_{f\beta} + \frac{v_{f\beta}^*}{L_f} - \frac{\hat{v}_\beta}{L_f}\right) \tag{19}$$

It is decided that the candidate function of Lyapunov will be:

$$V_3 = \frac{1}{2}z_3^2 \tag{20}$$

There is a function (20) whose derivative is:

$$\dot{V}_3 = z_3\left(i_{f\beta}^* - \left(-\frac{R_f}{L_f}i_{f\beta} + \frac{v_{f\beta}^*}{L_f} - \frac{\hat{v}_\beta}{L_f}\right)\right) \tag{21}$$

System stability is ensured when the Lyapunov function's derivative is negative; Guaranteeing system stability is as simple as selecting the derivative z_3 of as:

$$\dot{z}_3 = -k_3 z_3 \tag{22}$$

Wherek_3 presents a gain positive.

Equation (23) gives the resulting control law, and Fig. 4. shows its block diagram.

$$v_{f\beta}^* = L_f i_{f\beta}^* + L_f k_3 z_3 + R_f i_{f\beta} + \hat{v}_\beta \tag{23}$$

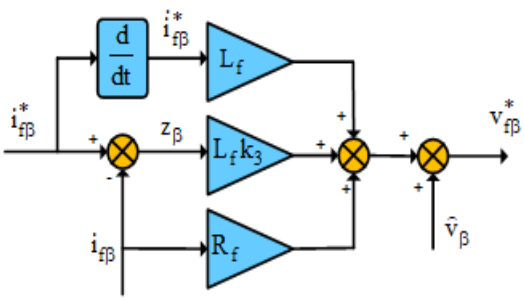

Fig. 4. Schematic of the NIBC of current $i_{f\beta}$

3.2. NIBC on the Boost Converter Side

The DC-DC converter is governed using a backstepping control strategy to ensure optimal energy harvesting from the PV source. The PV generator's output voltage and current are controlled by two NIBCs in the control system shown in Fig. 5. To accomplish voltage control, the MPPT algorithm supplies a reference value V_{pv}^* and uses it to regulate the PV generator voltage V_{pv}. The reference current for internal current regulation, the reference value I_{Lpv}^* is computed by integrating the voltage controller's output with a correction factor linked to the PV current.

In addition, as seen in Fig. 5, the DC/DC converter's duty cycle reference D^* is determined using the output of the current controller with compensation.

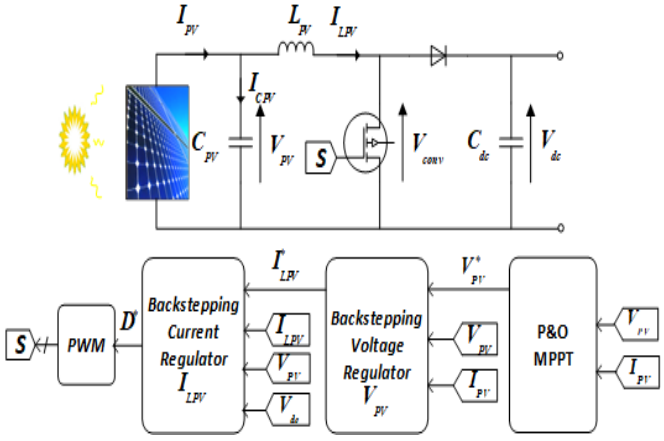

Fig. 5. Schematic of DC-DC converter NIBC.

Following the division of the global model provided by Equation (20) into two parts, the following NIBC controllers are utilised for the control of the system on the DC-DC converter side:

- **Part 1**

$$\frac{dV_{PV}}{dt} = \frac{1}{C_{PV}} I_{PV} - \frac{1}{C_{PV}} I_{LPV} \tag{24}$$

In this initial part of the control scheme, the current I_{LPV} is regarded as the fluctuating control input, and the corresponding output is the voltage produced $V_{PV}$by the PV generator.

- **Part 2**

The PV current $I_{LPV}$is the output variable in the second subsystem described by Equation (25), while the duty cycle D is the control variable.

$$\frac{dI_{LPV}}{dt} = \frac{1}{L_{PV}} V_{PV} - \frac{1}{L_{PV}} (1 - D) V_{dc} \tag{25}$$

3.2.1. Design of the NIBC voltage regulator

The synthesis of the voltage V_{PV} regulator utilising the backstepping technique, as shown by the first subsystem specified by Equation (24), is examined in this manner:

The tracking error variable $z_{Vpv}$is given by

$$z_{Vpv} = V_{PV}^* - V_{PV} \tag{26}$$

The dynamics of errors $z_{Vpv}$are supplied by:

$$\dot{z}_{Vpv} = \dot{V}_{PV}^* - \left(\frac{1}{C_{PV}} I_{PV} - \frac{1}{C_{PV}} I_{LPV}^*\right) \tag{27}$$

We select the candidate Lyapunov function as:

$$V_{Vpv} = \frac{1}{2} z_{Vpv}^2 \tag{28}$$

The function's (28) derivative is:

$$\dot{V}_{Vpv} = z_{Vpv}\left(\dot{V}_{PV}^* - \left(\frac{1}{C_{PV}} I_{PV} - \frac{1}{C_{PV}} I_{LPV}^*\right)\right) \tag{29}$$

Choosing the derivative z_{Vpv} of as follows will help to guarantee system stability: the Lyapunov function's derivative is negative.

$$\dot{z}_{Vpv} = -k_{Vpv} z_{Vpv} \tag{30}$$

Where k_{Vpv} is a gain positive.

Consequently, Equation (31) can be used to calculate the reference current. Fig. 6 shows its control schematic.

$$I_{LPV}^* = C_{PV} \dot{V}_{PV}^* - I_{PV} - k_{Vpv} C_{PV} (V_{PV}^* - V_{PV}) \tag{31}$$

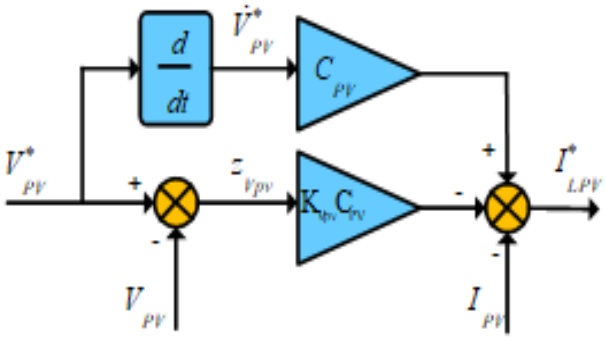

Fig. 6. Schematic of the NIBC of the voltage V_{PV}

3.2.2. Synthesis of the NIBC current regulator I_{LPV}

This is investigated by synthesising the required current regulation I_{LPV}PV using the second part defined by Equation (25).

The tracking error variable $z_{ILpv}$is defined as:

$$z_{ILpv} = I^*_{LPV} - I_{LPV} \tag{32}$$

The dynamics of the error z_{ILpv} is examined in this manner:

$$\dot{z}_{ILpv} = \dot{I}^*_{PV} - \left(\frac{1}{L_{PV}} V_{PV} - \frac{1}{L_{PV}}(1 - D^*)V_{dc}\right) \tag{33}$$

We select the candidate Lyapunov function as:

$$V_{ILpv} = \frac{1}{2} z^2_{ILpv} \tag{34}$$

The function's derivative Equation (34) is:

$$\dot{V}_2 = z_{ILpv}\left(\dot{I}^*_{PV} - \left(\frac{1}{L_{PV}} V_{PV} - \frac{1}{L_{PV}}(1 - D^*)V_{dc}\right)\right) \tag{35}$$

Choosing the derivative z_{ILpv} of as follows guarantees system stability:

$$\dot{z}_{ILpv} = -k_{ILpv} z_{ILpv} \tag{36}$$

Where k_{ILpv}denotes a gain positive.

Consequently, the duty cycle D^* may be computed via Equation (37). Fig. 7 illustrates the relevant control block diagram.

$$D^* = \frac{1}{V_{dc}}\left(L_{PV}\dot{I}^*_{LPV} - V_{PV} + V_{dc} + L_{PV} k_{ILpv} z_{ILpv}\right) \tag{37}$$

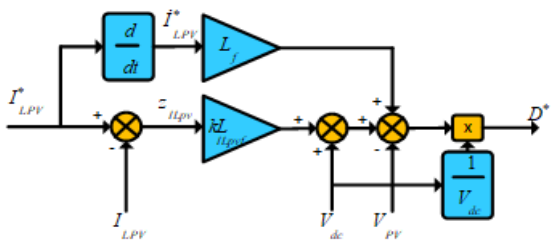

Fig. 7. Schematic of the NIBC control of the current I_{LPV}

4. The PIL Technique for Implementing Control Strategy

By immediately running the produced code on an embedded CPU in a real-time setting, the PIL test allows the validation and testing of regulation techniques, and it is a co-simulation approach. Here, we put the control algorithms through their paces in a real-world setting by simulating PIL operations on a C2000 LaunchXL-F28379D DSP board. Fig. 8 depicts the simulation setup, where the physical system model is executed on a host computer and constantly communicates with the embedded control algorithm running on the DSP board. In this configuration, important metrics like memory utilisation, code speed, and execution time may be optimised for a thorough evaluation of the system's behaviour [25–30].

To evaluate the real-time performance of the proposed diagnostic system, a PIL test was conducted. The system operated with a simulation time step of 1 ms, maintaining an average CPU load of 35 % (with peaks up to 55 %), and required approximately 120 kB of RAM and 450 kB of Flash memory. The measured host–target latency was around 250 µs, confirming the computational efficiency and suitability of the approach for real-time implementation.

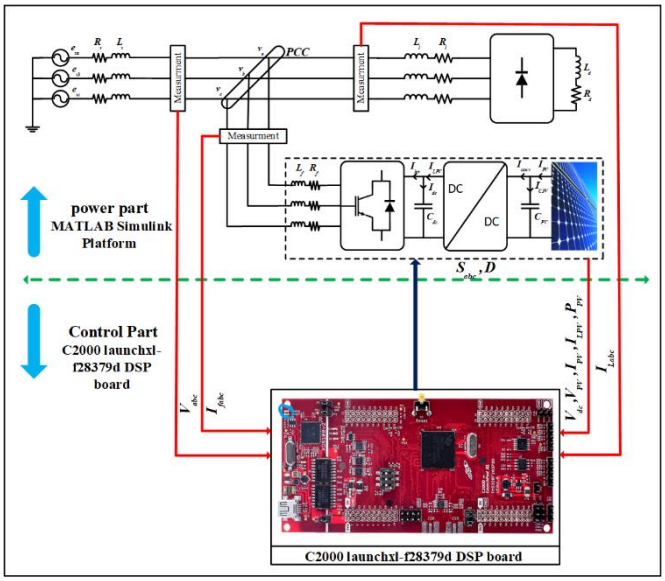

Fig. 8. Scheme of PIL.

5. Co-simulation Results and Discussion

The co-simulation of the PV-SAPF system controlled using the NIBC technique was carried out with the same parameters and under the same conditions mentioned earlier. The parameters of the BC controllers used are given in Table 1.

Table 1. Parameters of the BC-VOC-SVM controllers of the PV-SAPF system

SAPF Side	
DC bus voltage reference V_{dc}^{*}	700 V
DC-link capacitor C_{dc}	5 mF
Filter impedance R_f,L_f	1 mΩ, 350 µH
grid impedance R_l, L_l	2.7 mΩ, 26 µH
NIBC controller parameter for the DC bus voltage k_1	180
Parameters of the current $i_{f\alpha\beta}$controllerk_2, k_3	$5e^9$
Fundamental frequency f	50 Hz
switching frequencyf_{sw}	35 kHz
PV side	
Inductance L_{PV}	5 mH
Capacitance C_{PV}	55 mH
NIBC voltage V_{PV} controller parameter k_{Vpv}	$11010e^3$
NIBC current I_{LPV}controller parameterk_{ILpv}	$2e^3$

5.1. Variation in Solar Irradiance

Figs. 9 and 10 below show the results of the system's response to a change in solar irradiation under NIBC technique.

Fig. 9a shows the DC bus voltage waveform, which remains well-regulated at its reference value even during variations in solar irradiance. Fig. 9b displays the voltage and current waveforms of one grid phase, showing that they are in phase. The variation in the amplitude of source currents indicates the power level supplied or absorbed by the grid, as shown in Fig. 9c.

Moreover, the source current THD for phase a, obtained through Fast Fourier Transform (FFT) analysis, is 2.06%, which is well below the IEEE 519 recommended limit of 5%, as illustrated in Fig. 9d. This confirms that the proposed system effectively mitigates harmonic distortion and ensures compliance with international power quality standards.

Fig. 10 shows the PV generator's output power profile. In Fig. 10a, the PV output power follows the applied irradiance profile accurately. As the irradiance level increases, the PV output power rises accordingly, and the MPP shifts to track the new operating conditions. The active power produced by the PV system closely matches the maximum power of the PV generator under standard test conditions. The proposed control method exhibits a fast dynamic response, with a convergence time of approximately 0.002 s, and a steady-state error of about 40 W between the generated and reference PV power. These results demonstrate the high tracking efficiency and superior performance of the proposed control.

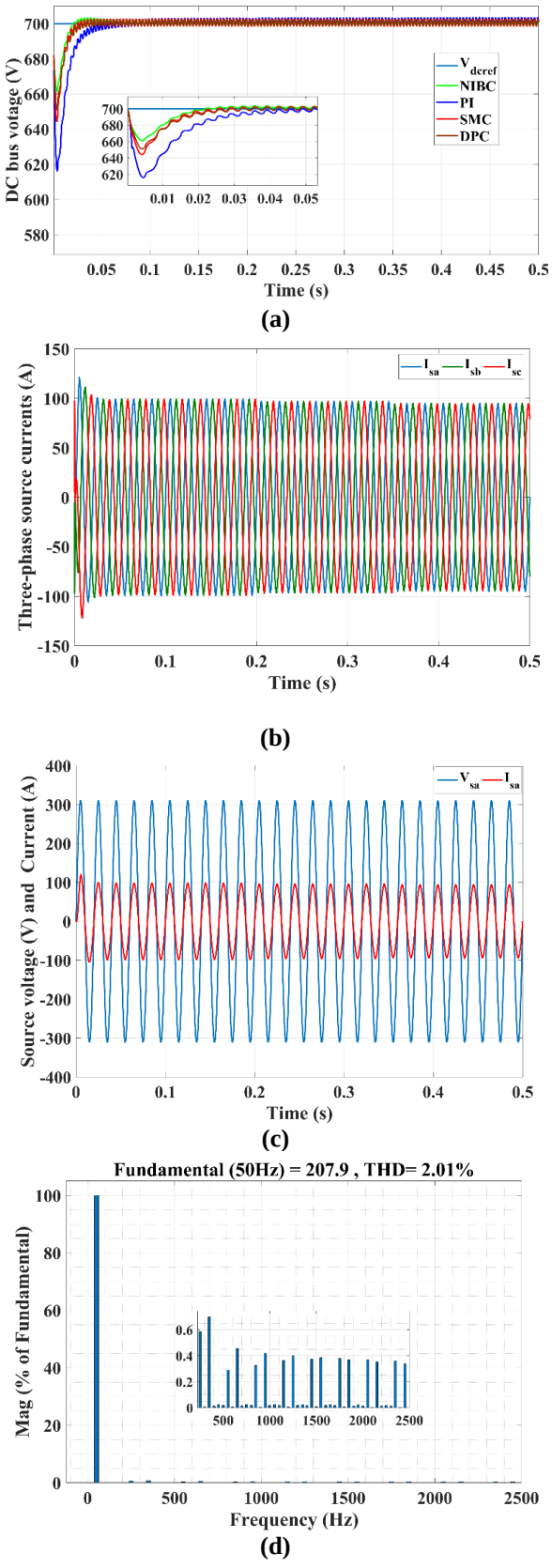

Fig. 9. Dynamic responses of the proposed system under changing solar irradiation (BC-VOC-SVM control): (a) the DC bus voltage V_{dc}, (b) a-b-c-phases currents of source I_{sabc} (c) Phase "a" of voltage $V_{sa}$and source current I_{sa}, and (d) Source current Harmonic spectrum.

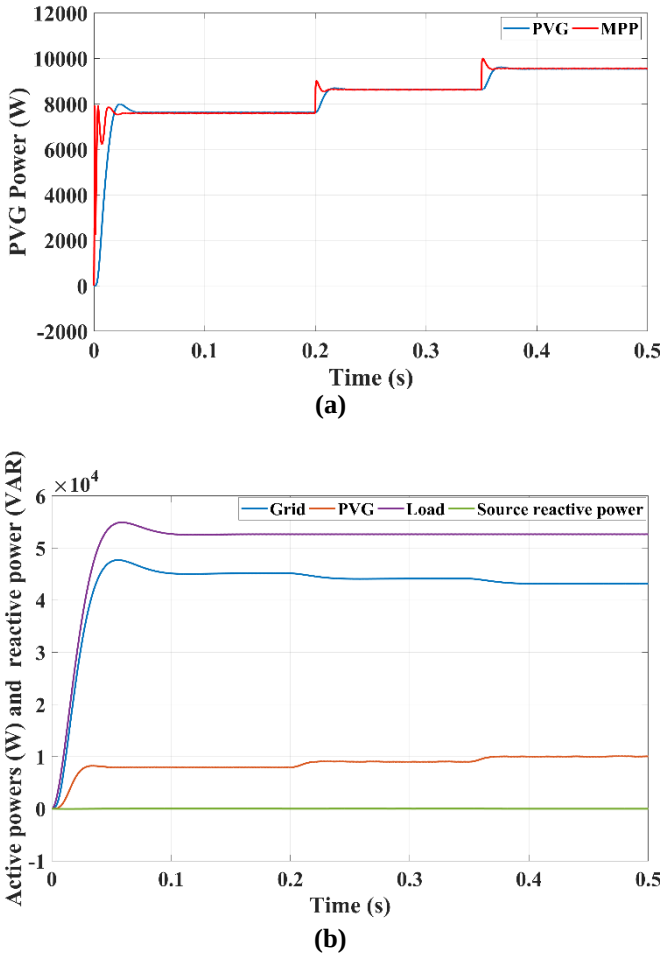

Fig. 10. Dynamic responses of the proposed system under changing solar irradiation (BC-VOC-SVM control): (a) GPV Power and its MPP, (b) Active powers of the grid P_s, the load P_L, and the VSI PF, Reactive powers of the grid Q_s, the load Q_L, and the VSI Q_F

5.2. Variation in Nonlinear Load

Figures 11 and 12 show the results of a nonlinear load variation under BC control of the PV-SAPF system.

The DC bus voltage remains stable at its reference value during abrupt changes in nonlinear load, as shown in Fig. 11a. Fig. 11b illustrates the grid phase current during load variation, showing that the sinusoidal shape of the current remains undistorted. This is reflected in the THD value, which is significantly reduced as shown in Fig. 11d. Fig. 11c also shows that the grid phase current remains in phase with its voltage during load changes, leading to a unity power factor on the grid side.

Fig. 12b shows the active power behavior: the inverter power always matches the PV generator power. As the load increases, grid power increases to compensate for the power shortfall from the PV generator. Meanwhile, the grid's reactive power remains zero. When the load's reactive power increases, the active filter provides the necessary reactive power in the opposite direction. Additionally, Fig. 12a shows that the PV generator's power continues to follow the irradiation profile, even when the load changes.

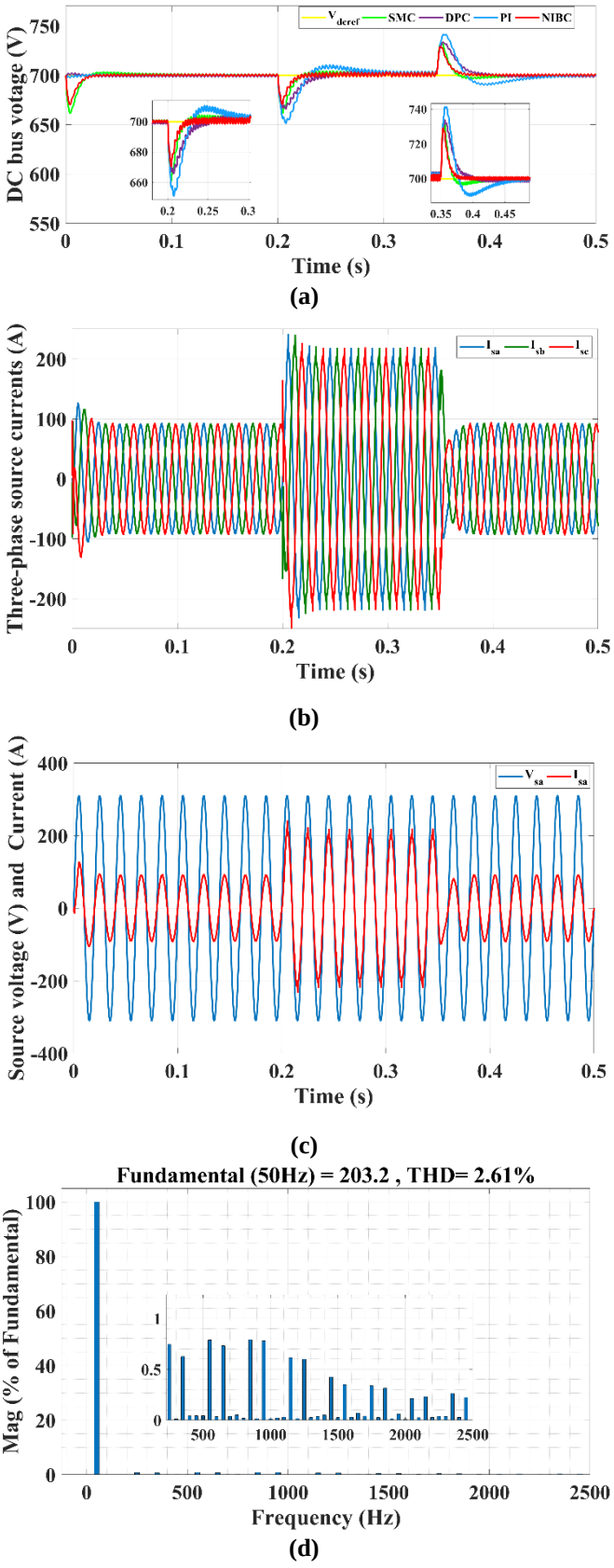

Fig. 11. Dynamic responses of the proposed system under changing solar irradiation (BC-VOC-SVM control): (a) the DC bus voltage V_{dc}, (b) a-b-c-phases currents of source I_{sabc} (c) Phase "a" of voltage V_{sa} and source current I_{sa}, and (d) Source current harmonic spectrum.

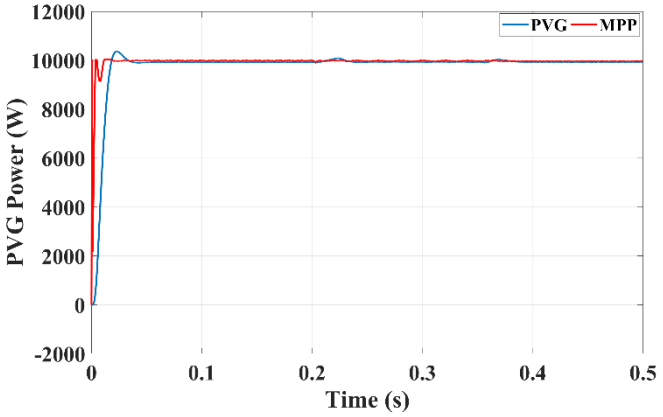

(a)

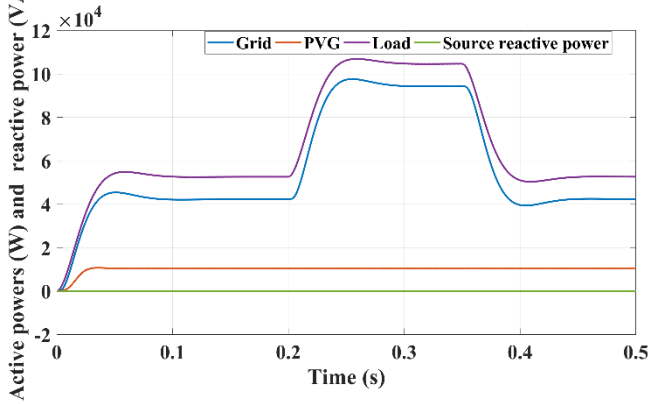

(b)

Fig. 12. System dynamic performance under nonlinear load disturbances with the proposed NIBC-VOC-SVM controller: (a) PVG power and its MPP and (b) Active powers of the grid P_s, the load P_L, and the VSI P_F, Reactive powers of the grid Q_s, the load Q_L, and the VSI Q_F

As seen in Table 2, the proposed NIBC controller achieves the lowest THD and fastest settling time, indicating superior dynamic and steady-state performance compared to other methods.

Table 2. Comparison between NIBC and conventional controllers under identical test conditions.

Controller	THD (%)	PF (%)	Overshoot (%)	Settling Time (ms)	Efficiency (%)
PI	3.5	92	7.14	14	89.35
SMC	3.75	89.5	5.46	6	94.784
DPC	3.18	95.3	4.43	7	96.383
NIBC (proposed)	**2.61**	**98.5**	**2.6**	**2.1**	**98.1**

5.3. Robustness Under Parameter Mismatch

Figs. 13 and 14 present the PIL validation results of the robustness test conducted to evaluate the system's performance under parameter uncertainties. The assessment considers deviations in the DC-link capacitor ($C = C_o$, $0.8\times C_o$, and $1.2\times C_o$) as depicted in Fig. 12, as well as variations in the filter inductance ($L = L_o$, $0.8\times L_o$, and $1.2\times L_o$) and resistance ($R = R_o$, $0.8\times$Ro, and $1.2\times R_o$), where C_o, L_o, and R_o denote the nominal parameters. The figure illustrates the DC-link voltage responses corresponding to a 700 V reference and the THD current under identical operating conditions to those described in Section 5.2.

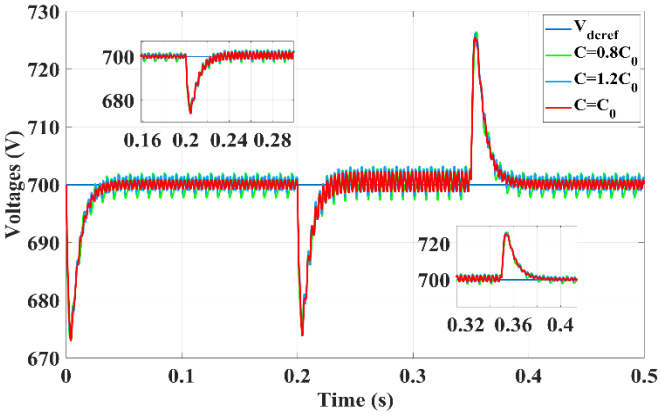

Fig. 13. DC-link voltage response under DC-link capacitor mismatch.

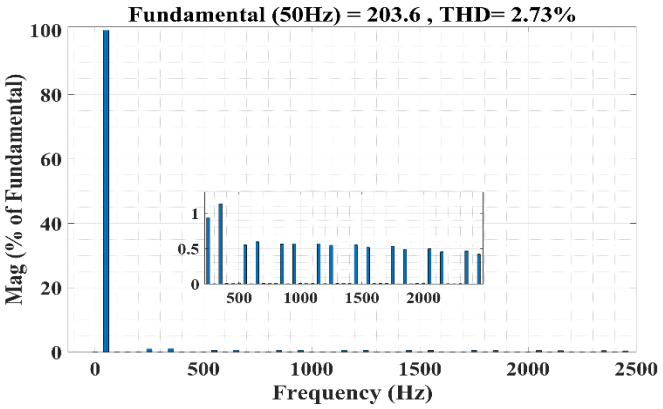

(a)

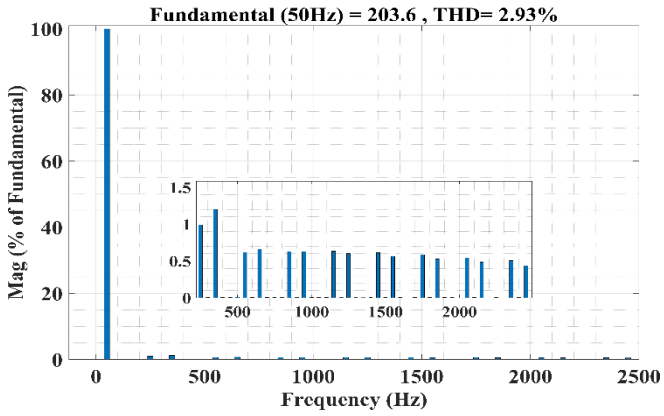

(b)

Fig. 14. Source current Harmonic spectrum response under filter inductance and resistance mismatch.

The obtained results confirm the remarkable robustness of the proposed control strategy, evidencing its strong

capability to accommodate parameter mismatches while maintaining stable operation and effective disturbance rejection throughout all operating scenarios.

5.4. Noise Assessment

To evaluate the robustness of the proposed NIBC technique against measurement noise, a simulation study was performed by introducing uniform random noise within the range of [-0.2 V, 0.2 V] to the measured DC microgrid voltage using the Uniform Random Number function. Fig.14 depicts the resulting DC microgrid voltage responses. Among the compared control methods—PI, SMC, and the proposed NIBC technique —the latter exhibits the best performance, showing a significant reduction in voltage drops and settling time while effectively suppressing measurement noise. Conversely, the conventional NIBC technique displays larger steady-state voltage ripples due to amplified noise effects. These results confirm that the proposed NIBC technique provides the most robust performance in mitigating measurement noise and rejecting external disturbances.

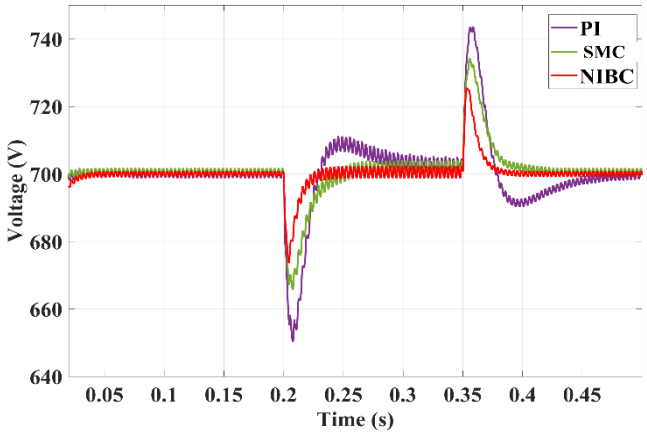

Fig. 15. DC-link voltage response with noise assessment.

6. Conclusions

This study presents an advanced control strategy for improving the performance and power quality of grid-connected PV systems, particularly in decentralized energy setups. The proposed approach integrates nonlinear ıntegral backstepping control with space vector pulse width modulation to optimize energy use, reduce SSEs, and enhance the control of key system parameters such as DC bus voltage, active and reactive power, and the maximum power point tracking process.

By utilizing a SAPF, the system ensures improved power quality, effectively minimizing THD values, maintaining a unity power factor, and achieving quick response times. This method also demonstrates strong resilience under varying solar conditions and load imbalances, with near-total elimination of steady-state faults. The system's stability and robustness have been validated through Lyapunov function analysis and Processor-in-the-Loop co-simulation results, confirming its ability to avoid overshooting and undershooting.

Overall, the integration of NIBC and SVPWM techniques enhances the efficiency, stability, and power quality of PV-micro grid-connected systems, making it a promising solution for modern smart grid applications.

In the future, the experimentally designed system will be implemented using real-world instruments, and the experimental results will be compared with other nonlinear strategies. Additionally, an attempt will be made to apply a fractional-order control strategy based on a neural algorithm to the NIBC approach in order to achieve high efficiency and superior operational performance for network-connected PV-micro systems.

Nomenclature

THD	Total harmonic distortion
PV	Photovoltaic system
PI	Proportional-integral controller
SMC	Sliding mode control
DPC	Direct power control
NIBC	Nonlinear ıntegral backstepping control
BC	Backstepping control
PVG	Photovoltaic generator
PIL	Processor-in-the-Loop
DSP	Digital Signal Processing
VSI	Voltage source inverter
VOC	Voltage-oriented control
MPP	Maximum power point
SSE	Steady-state error
SAPF	Shunt active power filter
P&O	Perturb and Observe
PAPF	Parallel active power filter
MPPT	Maximum power point tracking
SVPWM	Space vector pulse width modulation
NN	Neural network
PSO	Particle swarm optimisation
GA	Genetic algorithm

Acknowledgment

The authors would like to express their sincere appreciation to all contributors involved in this research. This work was conducted as part of a doctoral research project within the Electrical Engineering Laboratory of Guelma at the University of 8 May 1945, Guelma 24000. The authors gratefully acknowledge the academic environment, guidance, and support provided by the laboratory and the university, which greatly facilitated the completion of this study.

Author Contributions

Conceptualization, A. B., M. A., Z. L., and H. E. D.; methodology, A. B., M. A., Z. L., H.B. and H. E. D.; software, A. B., M. A., and Z.L.; validation, A. B., M. A., Z. L., and H. E. D.; formal analysis, A. B., M. A., Z. L., H. E. D., and H.B.; investigation, A. B., M. A., Z. L., and H.B., and H. E. D.; resources, A. B., M. A., H. B., Z. L., and H. E. D.; data curation, A. B., M. A., H. B., Z. L., and H. E. D.; writing-original draft preparation, A. B., M. A., Z. L., and H. E. D.; writing-review and editing, A. B., H. B., M. A., Z. L., and H. E. D.; visualization, A. B., H.B., M. A., Z. L., and H. E. D.; supervision, M. A., and H. E. D.; project administration, A.B., M.A., and H.B.;. All authors have read and agreed to the published version of the manuscript.

Conflict of interest

The author(s) declared no potential conflicts of interest with respect to the research, authorship, and/or publication of this article.

References

1. M. Osman and I. Qureshi, “Review of photovoltaic and concentrated solar technologies including their performance, reliability, efficiency and storage,” Results Eng., vol. 25, p. 104424, Mar. 2025, doi: 10.1016/J.RINENG.2025.104424.
2. S. M. Belhadj, B. Meliani, H. Benbouhenni, I. Colak, Z. M. S. Elbarbary and S. F. Al-Gahtani, "Control of three-level quadratic DC-DC boost converters for energy systems using various technique-based MPPT methods," Sci Rep vol. 15, pp. 14631, 2025. https://doi.org/10.1038/s41598-025-99551-2.
3. B. Maroua, Z. Laid, H. Benbouhenni, Z. M. S. Elbarbary, I. Colak, and M. M. Alammar "Genetic algorithm type 2 fuzzy logic controller of microgrid system with a fractional-order technique," Sci Rep vol. 15, pp. 6318, 2025. https://doi.org/10.1038/s41598-025-90239-1.
4. İ. F. Tepe, O. Taşdemir, and E. Irmak, “Design and Optimization of a Hybrid Energy Storage System Using the Dandelion Optimization Algorithm in Islanded Rural DC Microgrids,” 2025 13th International Conference on Smart Grid (icSmartGrid), pp. 249–257, May 2025, doi: 10.1109/icsmartgrid66138.2025.11071730.
5. M. N. Rahman, Md. S. Rahman, A. R. Rinatovich, M. M. Islam, V. Vavilov, and J. G. Singh, “Real-time energy management in microgrids using ARIMA Price forecasting and SLSQP optimization,” 13th International Conference on Smart Grid (icSmartGrid), pp. 310–316, May 2025, doi: 10.1109/icsmartgrid66138.2025.11071810.
6. H. Fatma-Zohra, D. Boukhetala, N. Debdouche, B. Habib, B. Jean-Pierre and L. Zarour, "Performance evaluation of nonlinear control approaches for grid-connected PV systems includes a novel fractional-order terminal-super twisting approach," Energy Reports, vol. 12, pp. 5024-5043, December 2024. https://doi.org/10.1016/j.egyr.2024.10.059.
7. Ch. Ali, D. Mabrouk, S. Ihammouchen, N. Bizon, B. Habib, K. Abdelhalim, R. Toufik, B. Mohamed-Fouad," An enhanced active disturbance rejection control scheme for DC voltage regulation in photovoltaic grid-connected four-leg inverter using a sliding mode observer," IEEE Access, vol. 13, pp. 18623-18643, 2025. doi: 10.1109/ACCESS.2025.3533015.
8. A. A. M. Faizal, N. Dwivedi, M. Sivasubramanian, S. Marisargunam, K. Rajesh, and N. Janaki, ‘Enhanced microgrid performance using coupled inductor switched Z-Source boost converter and GOA-tuned RBFNN MPPT,’ Int. J. Smart Grid - IjSmartGrid, vol. 9, no. 2, pp. 59–70, June 2025.
9. A. Boussafa, R. Rabeh, M. Ferfra, and K. Chennoufi, “Experimental test of optimizing maximum power point tracking performance in solar photovoltaic arrays based on backstepping control and optimized by genetic algorithm,” Results Eng., vol. 23, p. 102746, Sep. 2024, doi: 10.1016/J.RINENG.2024.102746.
10. L. El Oussoul, A. Elhamdaouy, and A. Ait Madi, “A new MPPT control strategy based on a weighting mechanism: Enhancing efficiency in solar energy harvesting,” Results Eng., vol. 26, p. 104725, Jun. 2025, doi: 10.1016/J.RINENG.2025.104725.
11. S. Akagi, S. Kaburagi, K. Ishibashi, K. Okumura, and R. Maeda, “Evaluation of the impact of uncertainty on reactive power reduction through fixed power factor adjustment of PV systems in medium-voltage distribution networks,” 2024 13th International Conference on Renewable Energy Research and Applications (ICRERA), pp. 612–616, Nov. 2024, doi: 10.1109/icrera62673.2024.10815182.
12. J. K. Sapawat and M. Miyatake, “Integration of solar PV with existing grid system to test a Ni-Cd battery set for railway applications,” 2024 13th International Conference on Renewable Energy Research and Applications (ICRERA), pp. 673–678, Nov. 2024, doi: 10.1109/icrera62673.2024.10815529.
13. S. Palavali and R. Kiranmayi, ‘PV model parameters extraction using opposition-based learning flow direction algorithm’, Int. J. Renew. Energy Res. IJRER, vol. 15, no. 3, pp. 488–502, Sept. 2025.
14. S. Akagi, S. Kaburagi, K. Ishibashi, K. Okumura, and R. Maeda, “Evaluation of the impact of uncertainty on reactive power reduction through fixed power factor adjustment of PV systems in medium-voltage distribution networks,” 2024 13th International Conference on Renewable Energy Research and Applications (ICRERA), pp. 612–616, Nov. 2024, doi: 10.1109/icrera62673.2024.10815182.
15. A. J. Alqattan, F. Albasri, and S. A. Al-Mosawi, ‘Modeling and assessment of D-STATCOM in grid connected PV system using ANN and ANFIS

controller', Int. J. Renew. Energy Res. IJRER, vol. 15, no. 3, pp. 525–536, Sept. 2025.

16. Y. Izgheche, T. Bahi, and A. Lakhdara, 'Analysis of genetic and cuckoo search algorithms for MPPT in partial shaded', Int. J. Smart Grid - IjSmartGrid, vol. 8, no. 1, pp. 35–40, Mar. 2024.
17. A. B. Djilali, E. Bounadja, A. Yahdou, H. Benbouhenni, Z. M. S. Elbarbary, I. Colak and S. F. Al-Gahtani, "Enhanced variable step sizes perturb and observe MPPT control to reduce energy loss in photovoltaic systems," Sci Rep. 15, pp. 11700, 2025. https://doi.org/10.1038/s41598-025-95309-y.
18. H. Renaudineau, F. Donatantonio, J.-P. Martin, S. Pierfederici, and F. Meibody-Tabar, "A PSO-based global MPPT technique for distributed PV power generation," IEEE Trans. Ind. Electron., vol. 62, no. 2, pp. 1047–1058, Feb. 2015, doi: 10.1109/TIE.2014.2336600.
19. A. B. Djilali, A. Yahdou, E. Bounadja, H. Benbouhenni, D. Zellouma, and I. Colak, "Energy management of the hybrid power system based on improved intelligent perturb and observe control using battery storage systems," Energy Reports, vol. 11, pp. 1611–1626, Jun. 2024, doi: 10.1016/J.EGYR.2024.01.010.
20. N. Debdouche, A. Chebabhi, B. Habib, F.-Z. Hadjaidji, Z. M. S. Elbarbary and S. F. Al-Gahtani, "Synergetic simplified super-twisting algorithm control for stability enhancement of PV/BESS-based DC microgrid," Scientific Reports, vol. 15, 7392, 2025. https://doi.org/10.1038/s41598-025-92042-4
21. K. Boutaghane, H. Benbouhenni, N. Bennecib, Z. M. S. Elbarbary, I. Colak, and M. M. Alammar, "Using new control strategies to improve the effectiveness and efficiency of the hybrid power system based on the battery storage system," Sci Rep vol. 15, pp. 4730, 2025. https://doi.org/10.1038/s41598-025-88804-9
22. Kh. N. Khallouf, Z. Laid, B. Habib, N. Debdouche, Z.M.S. Elbarbary, "Adaptive fuzzy logic control for microgrid-connected hybrid photovoltaic/wind generation systems," Energy Reports, vol. 12, pp. 4741-4756, Dec 2024. https://doi.org/10.1016/j.egyr.2024.10.042.
23. J. Y. Lee, R. Verayiah, K. H. Ong, A. Ramasamy, and M. B. Marsadek, "Voltage oriented control and direct power control strategies in solving under and overvoltage conditions for heavy load application on Malaysian distribution representative network," Electr. Eng., vol. 103, no. 3, pp. 1597–1612, Jun. 2021, doi: 10.1007/S00202-020-01143-Y/METRICS.
24. Y. Zhang, J. Liu, H. Yang, and J. Gao, "Direct power control of pulsewidth modulated rectifiers without DC voltage oscillations under unbalanced grid conditions," IEEE Trans. Ind. Electron., vol. 65, no. 10, pp. 7900–7910, Oct. 2018, doi: 10.1109/TIE.2018.2807421.
25. H. E. Ghadbane, S. Barkat, A. Houari, A. Djerioui, H. Rezk, and M. Louzazni, "Optimal adaptive fractional order integral sliding mode controller-energy management strategy for electric vehicles based on bald eagle search algorithm," Int. J. Energy Res., vol. 2024, 2024, doi: 10.1155/2024/7844084.
26. T. Kamel, D. Abdelkader, B. Said, S. Padmanaban, and A. Iqbal, "Extended Kalman Filter based sliding mode control of parallel-connected two five-phase PMSM drive system," Electron. 2018, Vol. 7, Page 14, vol. 7, no. 2, p. 14, Jan. 2018, doi: 10.3390/ELECTRONICS7020014.
27. H. E. Ghadbane, S. Barkat, A. Djerioui, A. Houari, M. Oproescu, and N. Bizon, "Energy management of electric vehicle using a new strategy based on slap swarm optimization and differential flatness control," Sci. Reports 2024 141, vol. 14, no. 1, pp. 1–19, Feb. 2024, doi: 10.1038/s41598-024-53396-3.
28. H. E. Ghadbane, S. Barkat, A. Houari, A. Djerioui, H. Abdelhak, and T. Mesbahi, "A load following energy management strategy for a battery-supercapacitor hybrid power system implemented with a PIL co-simulation approach," Smart Grids Sustain. Energy, vol. 9, no. 2, pp. 1–15, Dec. 2024, doi: 10.1007/S40866-024-00214-4/TABLES/4.
29. H. E. Ghadbane, S. Barkat, A. Houari, A. Djerioui, and T. Mesbahi, "Energy management strategy for hybrid power system implemented with processor in the loop," Oct. 2022, Hal Open Science [Online]. Available: https://hal.science/hal-03934029
30. H. E. Ghadbane, and A. F. Mohamed, "Optimizing fuel economy in hybrid electric vehicles using the equivalent consumption minimization strategy based on the arithmetic optimization algorithm," Math., vol. 13, no. 9, p. 1504, May 2025, doi: 10.3390/MATH13091504.